ORIGINAL

Optimized Deformable Model-based Segmentation and Deep Learning for Lung Cancer Classification

Mamtha V Shetty[1], Jayadevappa D[2], and Satish Tunga[3]

[1, 2]*Department of Electronics & Instrumentation Engineering, JSS Academy of Technical Education, Bengaluru, VTU, India,*
[3]*Dept. of Electronics & Telecommunication Engineering, M S Ramaiah Institute of Technology, Bengaluru, VTU, India.*

Abstract : Lung cancer is one of the life taking disease and causes more deaths worldwide. Early detection and treatment is necessary to save life. It is very difficult for doctors to interpret and identify diseases using imaging modalities alone. Therefore computer aided diagnosis can assist doctors for the early detection of cancer very accurately. In the proposed work, optimized deformable models and deep learning techniques are applied for the detection and classification of lung cancer. This method involves pre-processing, lung lobe segmentation, lung cancer segmentation, Data augmentation and lung cancer classification. The median filtering is considered for pre-processing and the Bayesian fuzzy clustering is applied for segmenting the lung lobes. The lung cancer segmentation is carried out using Water Cycle Sea Lion Optimization (WSLnO) based deformable model. The data augmentation process is used to augment the size of segmented region in order to perform better classification. The lung cancer classification is done effectively using Shepard Convolutional Neural Network (ShCNN), which is trained by WSLnO algorithm. The proposed WSLnO algorithm is designed by incorporating Water cycle algorithm (WCA) and Sea Lion Optimization (SLnO) algorithm. The performance of the proposed technique is analyzed with various performance metrics and attained the better results in terms of accuracy, sensitivity, specificity and average segmentation accuracy of 0.9303, 0.9123, 0.9133 and 0.9091 respectively. J. Med. Invest. 69 : 244-255, August, 2022

Keywords **:** *Shepard Convolutional Neural Network, Water cycle algorithm, Sea Lion Optimization, deformable model, Bayesian fuzzy clustering*

INTRODUCTION

Lung cancer is the more life-threatening disease in the globe and it requires appropriate diagnosis at an early stage of disease. In case, lung cancers are not identified and have not diagnosis at an early stage, it reduces the survival rate among patients. Hence an effective analysis and diagnosis of cancer disease saves the people lives. Computed Tomography (CT) is one of the imaging modality used to diagnose the lung diseases. The categorization of lung tumor from CT images acts as an important function in many lung based clinical applications. The segmentation of lungs lobes in lung imaging modality needs a robust correction model. This correction model relies on a spatial forms assessment using 3D geodesic map illustrations for the initial segmentation. The image based segmentation and classification is carried out by analyzing the given image. A machine learning scheme, like support vector machines (SVMs) and deep learning techniques are employed for the diagnosis of lung cancers in medical field. The fundamental steps for performing lung cancer detection involves lung segmentation, feature extraction and disease classification of the affected region (1).

The lung lobes are typically independent anatomic portions of lungs that plays major function in diagnosis and classification of lung diseases. The proper localization of lobe segmentation in CT images often signifies a non-trivial process even for experts. Accordingly, a lung lobe segmentation scheme is appropriate to process effectively under certain clinical conditions. An automatic and effective lobe separation from CT images is not only offer the boundaries for further processing, but it yields segmented region for registration processes. The lobe segmentation process permits the lobe based extraction, and then provides an accurate estimate of post-operative lung process. Though various lung lobe segmentation software exists there are no lobar quantization assistance available in lung segmentation processing software. The manual segmentation of affected region from lung lobe images is not feasible due to the huge quantity of slices in CT images. An automatic lung cancer segmentation process effectively segment the affected region even with low contrast and variable appearance. In some cases, it is difficult to evaluate an accurate location even for specialists. At the diagnosis of lung cancer, several symptoms are deliberated. Lung cancer has symptoms like Difficulties in Coughing and Chest pain. Consequently, the necessity of emerging a technique to identify the cancerous disease in an initial stage is increasing (2). Numerous assessment methods have been established for lung cancer recognition using various classifiers, for instance, SVM, K-nearest neighbor (KNN) and Artificial Neural Network (ANN) (3). The SVM is a widespread valuable learning process that relies on statistical learning theory (4). Though, these methods are effective and can identify lung cancer at its progressive stages is still challenging, due to their complexity. An early detection of cancer can be useful in preserving the disease completely. The computer vision community have proposed various computerized schemes, which are robotically detect and classify the normal and unhealthy regions. Automation in lung cancer detection with Computer Assisted Diagnosis (CAD) tools helps radiologists in quick and effective diagnosis (5). Among the various methods, one of the key challenges in CAD model for lung cancer detection relies on the morphological disparities of CT images. Typically, these variations are obvious in images with different image modalities, like Magnetic Resonance Imaging (MRI), X-ray, CT and Positron

Received for publication November 9, 2021 ; accepted June 6, 2022.

Address correspondence and reprint requests to Jayadevappa D, Department of Electronics & Instrumentation Engineering, JSS Academy of Technical Education, Bengaluru, VTU, India. e-mail : djayadevappa@jssateb.ac.in

Emission Tomography (PET), but in case of lung regions various physiological disparities are exist even when the same image modality is utilized (6). Recently, deep learning approaches (7) have combined with the hand modeled feature extraction scheme into integrated robust training scheme for cancer classification. Deep learning techniques provides a great performance as compared to traditional segmentation and classification schemes (8, 9).

The main objective of the proposed work is to design and develop the WSLnO based deformable model for the classification of lung disease. This method consists of pre-processing using median filter, lung lobe segmentation by Bayesian Fuzzy clustering method, and lung cancer classification using proposed WSLnO based deformable model. This model is designed by modifying the dictionary based image segmentation technique. After this, the data augmentation process is carried out to augment the size of segmented region. Finally, the lung cancer classification process is carried out using ShCNN, which is trained by the proposed WSLnO algorithm and it is designed by the incorporation of WCA and SLnO. Moreover, the proposed method classified the lung cancer region as benign or malignant and malignant metastatic.

BACKGROUND

This section provides the review of various lung cancer segmentation and classification techniques along with its advantages and disadvantages. Yu, H *et al*. (10) designed an Adaptive Hierarchical Heuristic Mathematical Model (AHHMM) for detecting the lung cancer using medical images. This method has the ability to extract any complex feature, but it is unable to predict the lung cancer at an initial stage. Onur Ozdemir *et al*. (11) developed the 3-D CNN for performing lung cancer detection and diagnosis. Although, the effectiveness of detection performance was found better, but the convolutional design was not considered for detecting lung cancer. M. Attique Khana *et al*. (12) modelled contrast based integrated design for performing lung cancer classification. This method attained better classification rate even with complex datasets. However, the computational cost of this method was high. Suresh S *et al*. (13) devised the CNN for performing an effective lung cancer diagnosis. Here, the processing speed of this method was found high and also failed to analyze the optimal size of input patch for deep learning schemes in order to attain efficient detection outcome. Ilaria Bonavita *et al*. (14) modelled the hybrid CNN for classifying the lung cancer. Here, the lung cancer detection process is carried out by combining three dimensional CNN with end to end pipeline scheme. Moreover, this method attained less complexity, less time consumption and less error prone processing. But, this method is not suitable for real time applications. Pankaj Nanglia *et al*. (1) developed the hybrid classifier in order to classify the lung cancer. The hybrid classifier was designed by combining SVM classifier and neural network. Even though it attained better performance for the increased training samples, still, it maintains classification accuracy. Lokanath Reddy Chilakala and Gattim Naveen Kishor (15) designed the Optimal Deep Belief Network (ODBN) with hybrid optimization algorithm for performing lung cancer classification. In this method, prior to the lung cancer classification, the irrelevant features were removed in order to enhance the classification performance. But, this method failed to process with larger datasets. Lakshmanaprabu S.K *et al*. (16) presented an optimal deep neural network (ODNN) for lung cancer classification. This method classified the lung nodules as either benign or malignant using ODNN, which was trained using modified gravitational search algorithm (MGSA). Though training time of this method was low, but it was failed to consider optimal feature selection approaches for better results.

The main challenges faced during the analysis of lung cancer segmentation and classification is described as follows.

In AHHMM (10) technique, the lung cancer prediction was proposed, but this method did not consider hybridized heuristic mathematical model for predicting the lung cancer at the early stage. Thus, the challenge lies on expanding the AHHMM method in order to enhance the performance and predict the disease at an early stage.

In (11), CNN approach was proposed for the lung cancer diagnosis. However, this method failed to generate high quality realistic inappropriate lung nodule samples based on generative adversarial networks to train radiologists for learning discriminative features, and also for enhancing the diagnostic decision making on cancer image. In (12), ODNN was developed for analyzing the various diseases using lung images. However, this method failed to consider high dosage CT lung images with multi-classifier for the efficient cancer detection process. In (13), the contrast based integrated design was developed for classifying the lung cancers. The contrast based integrated model attained accurate performance but the computational complexity of this method was high. Thus, the challenge lies on reducing the computational time. In (14), the challenges of three dimensional CNN model rely on the incorporation of patient referral with the training as well as learning models for further improving the performance. But, the incorporation of these models can increase the computational complexity.

PROPOSED METHOD

3.1 Database Description

The database used for the proposed method is Lung Image Database Consortium image (LIDC-IDRI) (22), which was found by National Institutes of Health (FNIH). This dataset comprised of three modalities ; computed radiography, digital radiography and lung cancer screening of CT scans with annotated lesion. Moreover, the database was produced by the incorporation of eight medical imagining companies and seven clinical centers for 1018 cases.

Initially, the input image is fed into the pre-processed using median filter to remove the unwanted noise and other distortions present in the input CT image. In the next stage, the lung lobes are segmented from the filtered image using Bayesian fuzzy clustering (17), which helps to perform effective classification of cancerous region. After segmentation, cancerous regions are separated using proposed optimization based deformable model, namely WSLnO based deform-able model. Here, the deformable model is formed by modifying the dictionary based image segmentation model (18). Moreover, the proposed WSLnO algorithm is designed by assimilating water cycle algorithm (WCA) (19) and Sea Lion Optimization (SLnO) (20).

After that, the data augmentation process is performed to augment the size of segmented image. Finally, the cancer classification process is carried out using ShCNN, which is trained using developed WSLnO based deformable model+ShCNN. The entire process of the proposed method is depicted in figure 1.

Let F is the database with n images represented as,

$$F = \left\{P_1, P_2, .. P_k, ... P_n\right\}, \qquad (1)$$

where, P_k represents the k^{th} image in database, $n$indicates the total count of images.

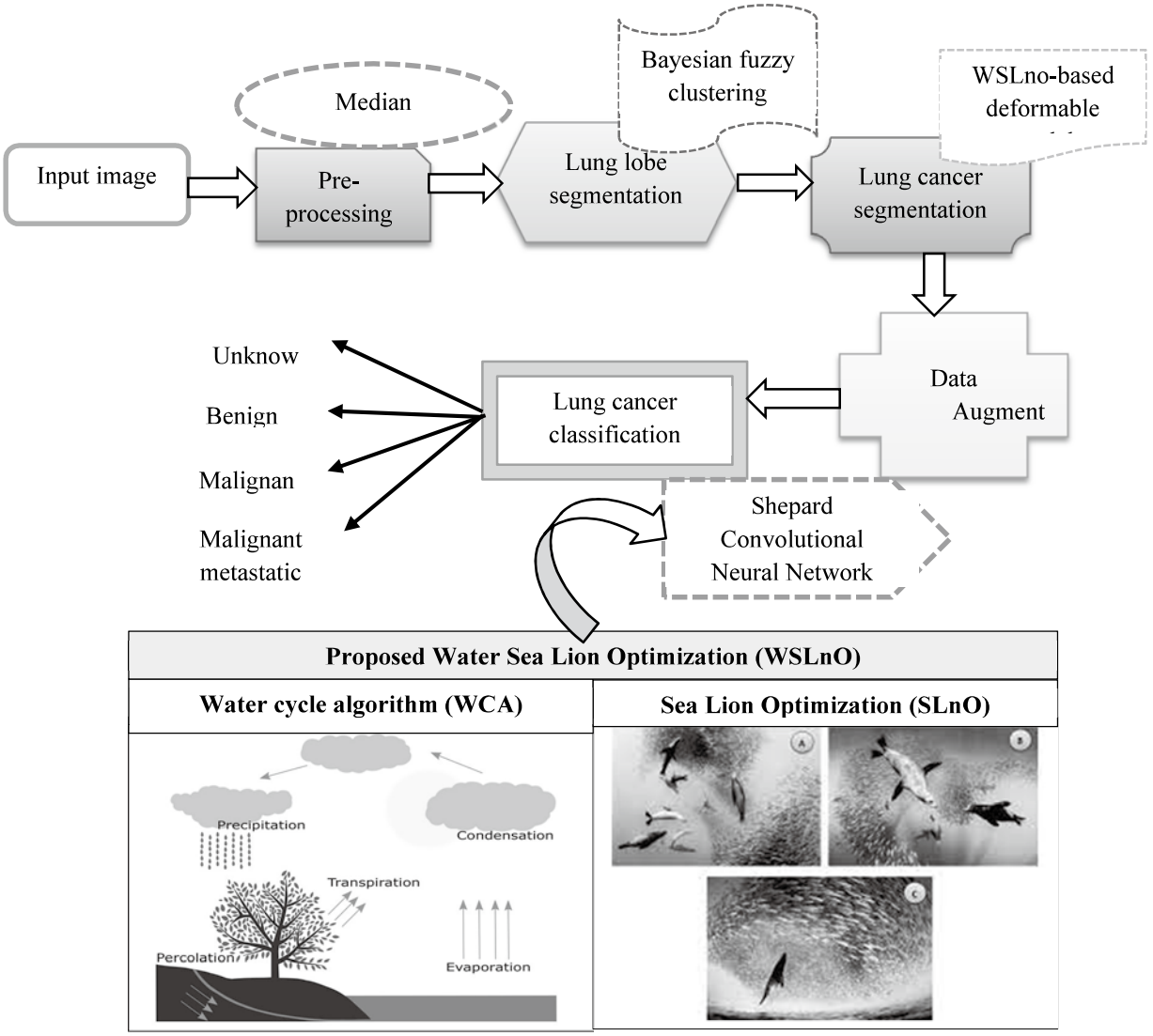

Figure 1. Block diagram of the proposed WSLnO-based Shepard Convolutional Neural Network for lung cancer classification.

3.2 Theory

In processing stage, the input image P_k is processed using median filter to remove the unwanted noise. This filtering technique has non-linear characteristics and is capable of eliminating the impulsive as well as salt and pepper noise which are common in CT images of the lungs. Moreover, the processing technique is also helps to preserve the edges of segmented image.

$$M(i,j) = median_{(W_1)\in Q_j}\left\{f(W_1)\right\} \qquad (2)$$

where, i and j are the image samples. The output of median filter is indicated as M_f.

3.2.1 Lung lobe Segmentation using Bayesian Fuzzy Clustering

The pre-processed image M_f is taken as an input of lung lobe segmentation, where the processing is carried out using Bayesian Fuzzy Clustering (BFC) approach. In lung lobe segmentation, the entire lung lobe regions are separated from the pre-proceed image. The direct segmentation of cancerous region from the pre-processed images will not provide an accurate results and there is a possibility of performing incorrect segmentation. Hence, the lung lobe segmentation is necessary to produce an accurate segmentation of lung cancer regions. The advantage of BFC scheme is that, the low computational complexity with accurate estimation. The BFC model is formed based on joint likelihood function for segmenting the lung lobe regions. Using BFC, the cancer affected by edema region is recognized without affecting the texture and edge of an image. Here, the cluster prototype is determined based on membership function and symmetric Dirichelet proposal g, which is expressed as,

$$g_x^+ \sim Dirichlet(P = 1_Z) \qquad (3)$$

where, g_x^+ specifies consistent symmetric Dirichlet proposal, and z denotes entire cluster count in segmentation process. Moreover, BFC utilizes conditional distribution and membership function for determining the cluster prototype. The expression for conditional distribution with membership function in BFC is given as,

$$\tilde{J}\left(B_u^t, g_x \middle| V\right) = \sum_{l=1}^{Z} \upsilon\left(B_u^t \middle| q_x, g_{xl}^{-V}\right) g_{xl}^{-V\upsilon/2}\, Dirichlet\left(q_u \middle| \varepsilon\right) \quad (4)$$

where, V specifies membership function, and q_x indicates the maximum-a-Posteriori sample. Also, the cluster prototype is determined based on Markov chain state rule, which is represented as,

$$J\left(B_u^t, g_x \middle| V\right) = J\left(B_u^t Y, g_x\right) J\left(g_x\right) \quad (5)$$

Thus, the maximum likelihood value of cluster prototype is considered as a final segmented result. Later, BFC technique calculates Z division for image slice B_u^t and is stated as,

$$S = \left\{S_1^{u,t}, S_2^{u,t}, ..., S_x^{u,t}, ..., S_Z^{u,t}\right\} \quad (6)$$

where, $S_x^{u,t}$ specifies x^{th} image segment B_u^t. The obtained sample of lung lobe segmentation is signified as, U.

3.2.2 Lung Cancer Segmentation using Proposed WSLnO-based Deformable Model

This method is based on dictionary based image segmentation and proposed WSLnO algorithm. In this case, the segmented lung lobe region U is considered as an input. Generally, deformable model defines the surface or curve exists inside the image, which has the ability to shift under the application of both internal and external forces. Moreover, deformable model expresses the geometric object whose shape can vary with time. Since, the traditional deformable model has the difficulties in processing object boundaries with concavities, the modified deformable model is formed by updating the equation of dictionary based image segmentation technique using proposed WSLnO algorithm. Thus, this model is designed by the incorporation of WCA and SLnO algorithm.

3.2.2.1 WSLnO Algorithm

The proposed WSLnO algorithm is modelled by the assimilation of WCA and SLnO algorithm for lung cancer segmentation. SLnO algorithm is formed by adapting the hunting activities of Sea Lions. Sea Lions have the better ability to detect the prey. Moreover, the SLnO algorithm has maximum local optimal solution and maximum convergence rate. The WCA algorithm is designed by adapting the process of water cycle, river flow as well as stream flow. WCA algorithm solves numerous optimization problems and attains maximum accuracy. Also, the computational complexity and searching behaviour of this algorithm was low. In order to overcome this limitation and to perform better segmentation, the WCA is integrated with SLnO algorithm. The steps of the proposed algorithm is as follows.

Step1 : *Initialization*

For evaluating the population-based optimization problems, the problem variables are needed to arrange in an array and the array is represented as,

$$K = \{K_1, K_2, \cdots, K_r, \cdots K_D\}; 1 \le r \le D \quad (7)$$

In order to initialize the optimization problem, the population of rain drops are organized in the matrix form, which is given by,

$$Population\ of\ \ Raindrop = \begin{bmatrix} P_{R1} \\ P_{R2} \\ P_{R3} \\ \vdots \\ R_{D_{pop}} \end{bmatrix} \quad (8)$$

$$Population\ of\ Raindrop = \begin{bmatrix} K_1^1 & K_2^1 & \cdots & K_{D_{\text{var}}}^1 \\ K_1^2 & K_2^2 & \cdots & K_{D_{\text{var}}}^2 \\ \vdots & \vdots & \vdots & \vdots \\ K_1^{D_{pop}} & K_2^{D_{pop}} & \cdots & K_{D_{\text{var}}}^{D_{pop}} \end{bmatrix} \quad (9)$$

where, Z depicts the total count of raindrops population, and D_{pop} and D_{var} signifies rain drop count and design variable count, respectively.

Step 2 : *Fitness function Evaluation*

The fitness function is employed to determine the optimal solution by evaluating fitness value of every solution so that the fitness with minimum value is considered as a best solution, which is presented in equation (31).

Step 3 : *Cost estimation of Raindrop*

The rain drop cost is evaluated by making x_{pop}. The minimum rain drop cost is deliberated as sea and the residual cost values are deliberated as river. Thus, the rain drop stream from river to sea is characterized as,

$$D_s = total\ \ river\ count + \underbrace{1}_{sea} \quad (10)$$

After fitness computation, every rain drop cost calculation is needed, which is assumed below.

$$\delta_c = f\left(C_1^c, C_2^c, ...C_{D\text{var}}^c\right); c = 1, 2, ...D_{pop} \quad (11)$$

where, δ_c states the rain drop cost, D_{pop} depicts the rain drops quantity, and D_{var} indicates the design variables count.

Step 4 : *Flow intensity of sea and river Estimation*

For assigning the raindrops to sea and river based on the flow intensity, the following equation (12) is utilized.

$$xV_i = round\left(\left|\frac{\delta_i}{\sum_{i=1}^{x_C}\delta_i}\right| \times D_{raindrops}\right); i = 1, 2, ...D_s \quad (12)$$

where, xV_i depicts the quantity of streams, which drift to specific sea or rivers.

Step 5 : *Stream flow to river*

The water stream is formed from the river by combining the rain drops with one another. Among the entire river, some of them are directly flow into the river. However, the ending point of all river should be linked with sea. The flow of streams to rivers is evaluated by,

$$K_{stream}^{r+1} = K_{stream}^r + rand\left(K_{river}^r - K_{sream}^r\right) \quad (13)$$

Step 6 : *River flow to sea*

The river stream to sea is evaluated using the solution update of WSLnO algorithm. The depiction of river flow to sea is evaluated using the equation given below,

$$K_{river}^{r+1} = K_{river}^r + rand\left(K_{sea}^r - K_{river}^r\right) \quad (14)$$

The above equation (14) can be rewritten as,

$$K_{stream}^{new} = K_{sea} + \sqrt{\sigma} \times rand(1, D_{\text{var}}) \quad (15)$$

Moreover, the performance of WCA can be enhanced by including the update equation of SLnO algorithm. Thus, the update equation of SLnO algorithm is given by,

$$K^{new} = R(s) - Dist.H \quad (16)$$

$$K^{new} = R(s) - \left|2G.R(s) - K\right|.H \quad (17)$$

Assuming $R(s) > K(s)$, then the expression becomes,

$$K_{new}^{stream} = R(s) - \left(2G.R(s) - K\right).H \quad (18)$$

$$K_{new}^{stream} = R(s)\left(1 - 2.G.H\right) + K.H \quad (19)$$

$$R(s) = \frac{K_{new}^{stream} - K.H}{1 - 2.G.H} \quad (20)$$

Substituting equation (20) in equation (15), then the expression becomes,

$$K_{stream}^{new} = \frac{K_{new}^{stream} - K.H}{1-2.G.H} + \sqrt{\sigma} \times rand\,d(1,\ D_{\text{var}}) \quad (21)$$

$$K_{stream}^{new} = \frac{K_{new}^{stream}}{1-2.G.H} - \frac{K.H}{1-2.G.H} + \sqrt{\sigma} \times rand\,d(1,\ D_{\text{var}}) \quad (22)$$

$$K_{stream}^{new} - \frac{K_{new}^{stream}}{1-2.G.H} = \sqrt{\sigma} \times rand\,d(1,\ D_{\text{var}}) - \frac{K.H}{1-2.G.H} \quad (23)$$

$$K^{new}\left(1 - \frac{1}{1-2.G.H}\right) = \sqrt{\sigma} \times rand\,d(1,\ D_{\text{var}}) - \frac{K.H}{1-2.G.H} \quad (24)$$

$$K^{new}\left(\frac{1-2.G.H+1}{1-2.G.H}\right) = \sqrt{\sigma} \times rand\,d(1,\ D_{\text{var}}) - \frac{K.H}{1-2GH} \quad (25)$$

$$K^{new} = \frac{2.G.H-1}{2.G.H}\left[\sqrt{\sigma} \times rand\,d(1,\ D_{\text{var}}) - \frac{K.H}{1-2.G.H}\right] \quad (26)$$

here, equation (26) represents the final updated equation of WSLnO algorithm.

where, σ=0.1, G=[0,1], H diminished linearly from 2 to 0, K represents the position vector of sea lion, *rand d* states uniformly distributed random integer, which lies between [0, 1].

Step 7 : *Exchange River location*

If the position of stream is better than the river position, then the river and stream exchange their positions, which signifies that the river is transformed into stream and vice versa. If the river finds the best location than the sea, then the river location is replaced with sea.

Step 8 : *Evaporation rule*

Photosynthesis is the process of transforming the water from stream and river to cloud in the atmosphere. When the temperature is reduced in the atmosphere, then the cloud cools down and back to earth in the form of rain. This cyclic process forms a new river or stream flow into the sea, and is termed as water cycle. The expression for evaporation is given by,

$$\left|K_{sea}^{r} - K_{river}^{r}\right| < \beta_{\max} \quad ;r = 1,2,3,...l_{V} - 1 \quad (27)$$

If the above condition satisfies, then the water cycle initialized, where, β_{max} is a small integer, which is close to zero.

Step 9 : *Raining process*

After the satisfaction of evaporation rule, the raining process initiates. This raining process forms the new stream flow in various locations. The new position of newly formed streams is assumed by,

$$K_{srteam}^{new} = B_L + rand \times \left(B_U - B_L\right) \quad (28)$$

where, B_L and B_U shows lower bound and upper bound. Moreover, computational as well as convergence rate is improved and the stream is straightly flow into sea, which is given by

$$K_{stream}^{new} = K_{sea} + \sqrt{\sigma}\, rand\, d\left(1, D_{\text{var}}\right) \quad (29)$$

where, σ agrees a coefficient, and it establishes the range of region near sea, *rand d* signifies randomly distributed integer.

Step 10 : *Decrement the value of user defined constraint*

The large amount of β_{max} reduces a searching ability, but less value assists search intensity close to sea. The value of β_{max} is decrement by,

$$\beta_{\max}^{r+1} = \beta_{\max}^{r} - \frac{\beta_{\max}^{r}}{v} \quad (30)$$

where, v signifies the maximum iteration.

Step 11 : *Feasibility solution Evaluation*

The optimal solution is evaluated using equation (31), and if a new solution is optimal than earlier solution then updates an earlier value with new optimal one.

Step 12 : *Termination*

The mentioned steps are repeated till the optimal solution is reached.

3.3 Optimized Dictionary based Image Segmentation

The optimized dictionary based image segmentation model is described as below.

Region dependent curve evolution : Let us consider an image A with its object and background is differentiated using two mean label densities x_{out} and x_{in}. Here, the curve is calculated for segmenting an image. When the pixel intensities are close to x_{out}, then the curves are diminished. When the pixel intensities are close to x_{in}, then the curves are enlarged. Moreover, the threshold of reduction and enlargement is measured as $(x_{in}+x_{out})/2$. The curve of an image is initialized using zero level evolution, which is specified by,

$$\frac{\partial \rho}{\partial x} = \varpi_{\in}(\rho)\left[\left(x_{out} - x_{in}\right)\left(2A - x_{out} - x_{in} + b_n\right)\right] \quad (31)$$

where, b indicates the minimum curve length, $_n$ indicates the level set curvature. The expression for curve length b is termed as,

$$b = \nabla.\left(\frac{\nabla \rho}{|\nabla \rho|}\right) \quad (32)$$

Texture dictionary : Here, the patches of an image with dimension $I \times I$ is extracted and gathers the pixels intensities in patch vector of $x \times I^2$ length. The group of patches are determined using Euclidean distance and k-means approach in order to create dictionary. The patches of all images are assigned into a single dictionary and the entire pixel of an image is based on $x = I^2$ such that the image patches are overlapping. Moreover, the binary relation between image and dictionary pixels is represented using sparse binary matrix X with $|\Omega|$ rows and dx columns. Here, $|\Omega|$ represents the total count of pixel in an image and dx indicates the total count of dictionary pixels in an image. Here, matrix X collects the texture minutiae of image based on two encodings, like spatial relationship among patches as well as dictionary task of entire patches.

Label to Probability Transformation : Every patch of an image A has an equivalent patch label. The image patches exist in entire dictionary units, which is utilized to estimate the dictionary component labels. The dictionary label is estimated based on the multiplication of binary vector S_{in} with X, which is represented as,

$$f_{in} = diag\left(X_1\right)^{-1} Xs_{in} \quad (33)$$

The parameter f_{in} is needed to rearrange based on the dimension of dictionary in order to attain dictionary label. Moreover, the probability transformation is determined based on the probability of an image pixel from dictionary labels.

To calculate the pixel probability, x values are essential to average due to the patch overlapping.

$$T_{in} = diag\left(X_1^{I}\right)^{-1} X^{I} \tilde{f}_{in} \quad (34)$$

The binary values from S_{in} is diffused based on the texture details encoded in X.

Multiple labels : The image labels with s_1 to s_E layers are created for handling multiple layers. The transformation is subjected to all layers, thereby dictionary labels become g_1 to g_x, and its normalization function is represented as,

$$\left(\tilde{f}_1, \tilde{f}_2, ..., \tilde{f}_E\right) = \frac{1}{M}\left(\frac{f_1}{|\Omega_1|}, \frac{f_2}{|\Omega_{21}|}, ..., \frac{f_E}{|\Omega_E|}\right) \quad (35)$$

$$M = \sum_{e=1}^{E} \frac{f_E}{|\Omega_E|} \quad (36)$$

After the completion of area normalization, the transformation is subjected to entire $\tilde{f}_E$.

Curve evolution : The closed curve is represented as zero level

set of function ρ, which expresses label image S_{in} attains 1, while ρ is negative or else it is zero. The expression for curve evolution is stated as,

$$\frac{\partial \varphi}{\partial x} = \frac{1}{2} - T_{in} + b_n \left| \nabla \rho \right| \tag{37}$$

The pixel wise transformation probability for all labels are stated as,

$$\left(\tilde{a}_1, \tilde{a}_2, ...\tilde{a}_E\right) = \left(\begin{array}{c} \dfrac{a_1}{a_1 + \max\left(a_w\right)}, \dfrac{a_2}{a_2 + \max\left(a_w\right)}, ..., \\ w \neq 1 \qquad\qquad w \neq 2 \\ \dfrac{a_E}{a_E + \max\left(a_w\right)} \\ w \neq E \end{array} \right) \tag{38}$$

here, the multi-label segmentation of level set solution is represented as,

$$\frac{\partial \rho_e}{\partial x} = \frac{1}{2} - \tilde{T}_e + b_n \left| \nabla \rho_e \right| \qquad ; e = 1, 2, ..., E \tag{39}$$

Moreover, the curve updation is carried out by,

$$\rho^{x+1} = \rho^x + \Delta x \frac{\partial \rho}{\partial x} \tag{40}$$

From WSLnO, the curve updation equation is given by,

$$K^{new} = \frac{2.G.H-1}{2.G.H} \sqrt{\sigma} \times rand\, d(1, D_{\text{var}}) - \frac{2.G.H-1}{2.G.H} \times \frac{K.H}{1-2.G.H} \tag{41}$$

$$K^{new} = \frac{2.G.H-1}{2.G.H} \sqrt{\sigma} \times rand\, d(1, D_{\text{var}}) + \frac{K}{2.G} \tag{42}$$

$$K = \left[K^{new} - \frac{2.G.H-1}{2.G.H} \sqrt{\sigma} \times rand\, d(1, D_{\text{var}}) \right] \times 2G \tag{43}$$

The above equation (43) can be rewritten as,

$$\rho = \left[\rho^{x+1} - \frac{2.G.H-1}{2.G.H} \left(\sqrt{\sigma} \times rand\, d(1, D_{\text{var}}) \right) \right] \times 2G \tag{44}$$

Substitute equation (44) in equation (40), then the equation becomes,

$$\rho^{x+1} = \rho^{x+1} \times 2G - \frac{2.G.H-1}{2.G.H} \left(\sqrt{\sigma} \times rand\, d(1, D_{\text{var}}) \right) \times 2G + \Delta x \frac{\partial \rho}{\partial x} \tag{45}$$

$$\rho^{x+1} - \rho^{x+1} \times 2G = \frac{1-2.G.H}{H} \left(\sqrt{\sigma} \times rand\, d(1, D_{\text{var}}) \right) + \Delta x \frac{\partial \rho}{\partial x} \tag{46}$$

$$\rho^{x+1} \left(1 - 2G\right) = \frac{1-2.G.H}{H} \left(\sqrt{\sigma} \times rand\, d(1, D_{\text{var}}) \right) + \Delta x \frac{\partial \rho}{\partial x} \tag{47}$$

$$\rho^{x+1} = \frac{1}{1-2G} \left[\frac{1-2.G.H}{H} \left(\sqrt{\sigma} \times rand\, d(1, D_{\text{var}}) \right) + \Delta x \frac{\partial \rho}{\partial x} \right] \tag{48}$$

here, the segmented outcome of cancer image is represented as Σ, which is forwarded to the data augmentation phase in order to enlarge the size of segmented cancer image.

3.4 Data Augmentation

Data augmentation process is carried out to enlarge the size of segmented image for performing effective classification. This process consists of random rotation, resizing and flipping. Each of these three processes performs separate operations for enlarging the images. The first step involved in the data augmentation process is random rotation.

Random Rotation : Random rotation is a valuable augmentation step in particular since it adjusts the angles of objects appears in the image. For performing random rotation, the images are gathered in horizontal direction but the resultant of random rotation, the object appears in any direction. The advantage of random rotation model is to improve the classification performance and avoids the over fitting issue.

Resizing : The second step involved in the data augmentation process is resizing. The resizing process adjusts the size of segmented image as required for further processing.

Flipping: Third step involved in the data augmentation process is flipping. The flipping phase flips the image as either horizontal or vertical direction. The output obtained from the data augmentation process is represented as L.

3.5 Lung Lesion Classification using Proposed WSLnO-based ShCNN

The augmented image L is considered as an input of ShCNN for lung cancer classification. The lung cancer classification is carried out using ShCNN where the weight of ShCNN is trained using WSLnO algorithm. The advantage of using ShCNN classifier is that, this classifier is effective and it provides an accurate classified outcome. Moreover, the processing speed of this method is high. The proposed WSLnO algorithm is designed by the incorporation of WCA and SLnO.

3.5.1 ShCNN architecture

The ShCNN model (21) is an extension of CNN. The purpose of designing Shepherd framework model is to resolve the issues of conventional interpolation layer for enhancing the network structure. The advantage of ShCNN is that, the processing time and computational complexity of this method is low. The ShCNN is designed by applying the Shepard interpolation layer with traditional CNN. In Shepard model, the known pixels are represented as weights, which varies based on spatial distance to processed pixel. Here, the ShCNN takes L as an input to classify the whether the lung cancer is benign, le, malignant metastatic or unknown. Hence, the Shepard model is expressed in convolution, which is given as,

$$M_{sh} = \begin{cases} \left(a * h\right)_{sh} / \left(a * y\right)_c & ; if\ y_{sh} = 0 \\ h_{sh} & ; if\ y_{sh} = 1 \end{cases} \tag{49}$$

where, h specifies input, M_{sh} states the output, c symbolizes image coordinates, y specifies binary indicator, y_{sh} denotes unknown pixel values, $*$ denotes convolution operation, and a represents kernel function. Moreover, the kernel function weight is inversely proportional to distance among the pixel with $y_{sh} = 1$ and pixel to functions. The element wise division among convoluted image as well as convolved mask is normally employed to handle the propagation of pixel information over the regions. Moreover, this method allows to handle the intermittently spaced information.

Shepard interpolation layer : The motive of inventing convolutional layer in the Shepard model is to create flexible function and to attain the kernel model in data driven form, and hence this layer is named as Shepard interpolation layer. Hence, the trainable interpolation layer is stated as,

$$z_k^m \left(z^{m-1}, y^m\right) = \lambda \left(\sum_l \frac{a_{kl}^m * z_l^{m-1}}{a_{kl}^m * y_l^m} + o^m \right); m = 1, 2, 3, . \tag{50}$$

where, m represents index of layers, z_k^m signifies feature map of k^{th} index in m^{th} layer, z_l^{m-1} shows l^{th} feature map at $(m\text{-}1)^{th}$ layer, z^{m-1} symbolizes the current layer input, which is the feature map of $(m\text{-}1)^{th}$ layer, y^m signifies the mask of present layer, and a_{kl} indicates trainable kernels, which is located in both the denominator and numerator of calculating fraction. Here, O means bias, and λ states nonlinearity of network. The term a_{kl} is convolved in activation of predecessor layer in numerator and the mask of present layer y^m in denominator. Here, y^{m-1} is the output gathered from CNN layer, which is obtained from either pooling or convolutional layer. The interpolation layers are primarily used to generate interpolation function with multiple count of nonlinearity layers. Here, mask indicates binary map, which carries the value of '1' for known region, and '0' for missing region.

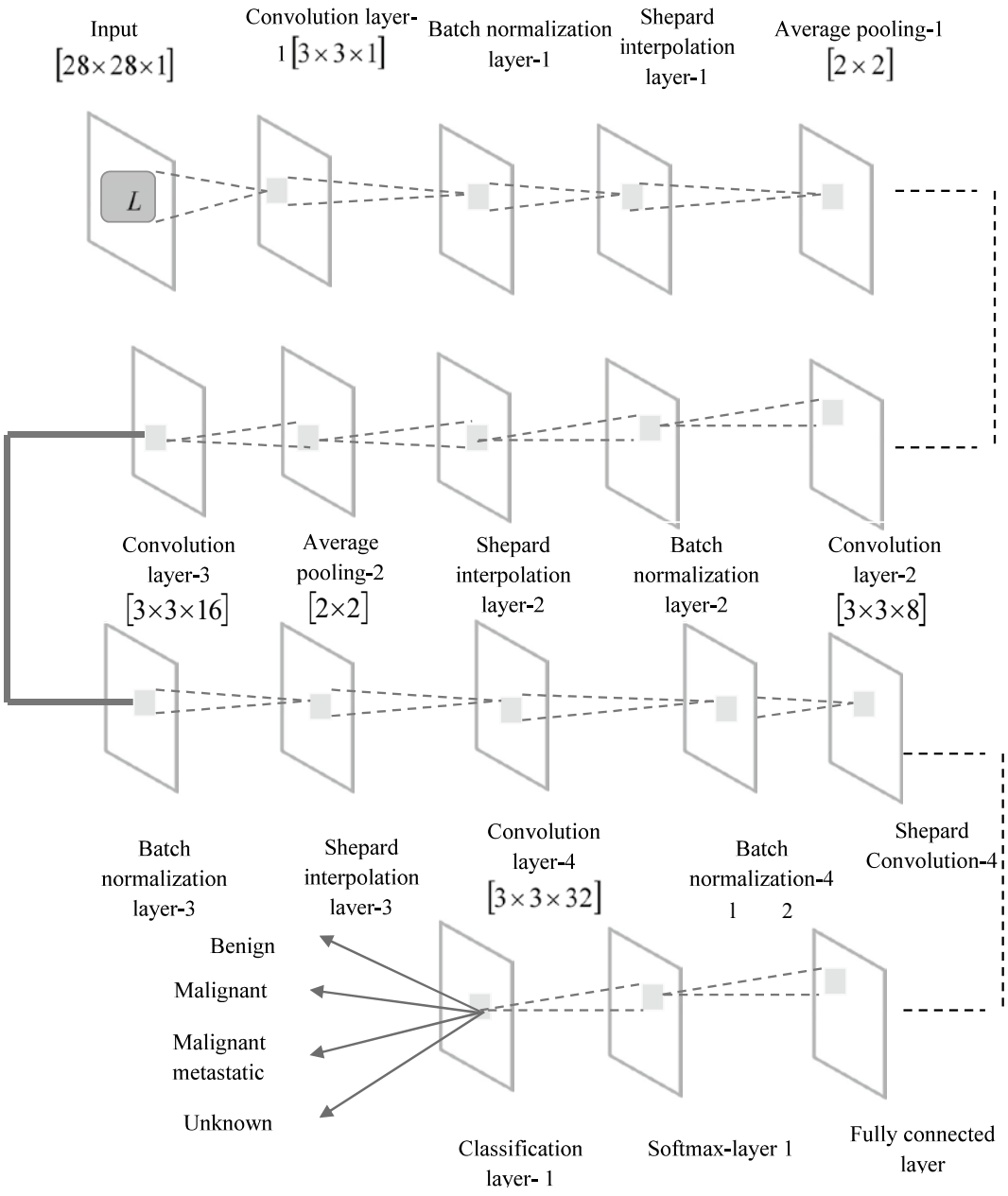

Figure 2. Design of Shepard Convolutional layer

Figure 3 demonstrates the structure of ShCNN. Thus, the ShCNN provides an effective classified outcome, which is represented as ω. The lung cancer classification is carried out using ShCNN, where the weights of ShCNN is trained using WSLnO based on fitness function given in equation (31). Moreover, the algorithmic process of WSLnO for training ShCNN is explained in the previous. Thus, the proposed WSLnO based ShCNN algorithm classifies the lung cancer disease as malignant, benign or malignant metastatic.

RESULTS

The performance assessment of the proposed model is evaluated using various performance metrics. The average segmentation accuracy is calculated by varying the cluster size for different iterations. Figure 4 illustrates the performance assessment of accuracy, sensitivity, specificity and average segmentation accuracy for different sizes of training data and cluster size. In figure 4(a), using 50% of training data, the accuracy calculated as 0.778, 0.785, 0.790, 0.807 and 0.833 for the iterations of 20, 40, 60, 80 and 100 respectively. Figure 4(b) shows the sensitivity values of 0.834, 0.853, 0.874, 0.881 and 0.894 for the 80% training data. Figure 4(c) shows the specificity values of 0.823, 0.841, 0.850, 0.863 and 0.813 for 70% training data. In figure 4(d), average segmentation accuracy of 0.806, 0.825, 0.862, 0.877 and 0.912 are presented for the cluster size 6.

4.1 Performance Metrics

The performance metrics used to evaluate the proposed WSLnO based deformable model for lung cancer classification are as follows.

$$AverageSegmentation(S_a) = \frac{K+L}{K+L+M+N} \quad (51)$$

where, K specifies true positive rate, L states true negative rate, M denotes false positive rate and N represents false negative.

$$Sensitivity(S_e) = \frac{N}{N+M} \quad (52)$$

$$Specificity(S_p) = \frac{M}{M+N} \quad (53)$$

Figure 3 shows the experimental results of lung cancer segmentation process. Figure 3(a) represents three sampled input CT images are used for the experimental purpose. Figure 3(b) represents the filtered images, figure 3(c) shows the lobe segmented regions and figure 3(d) indicates the segmented cancerous regions.

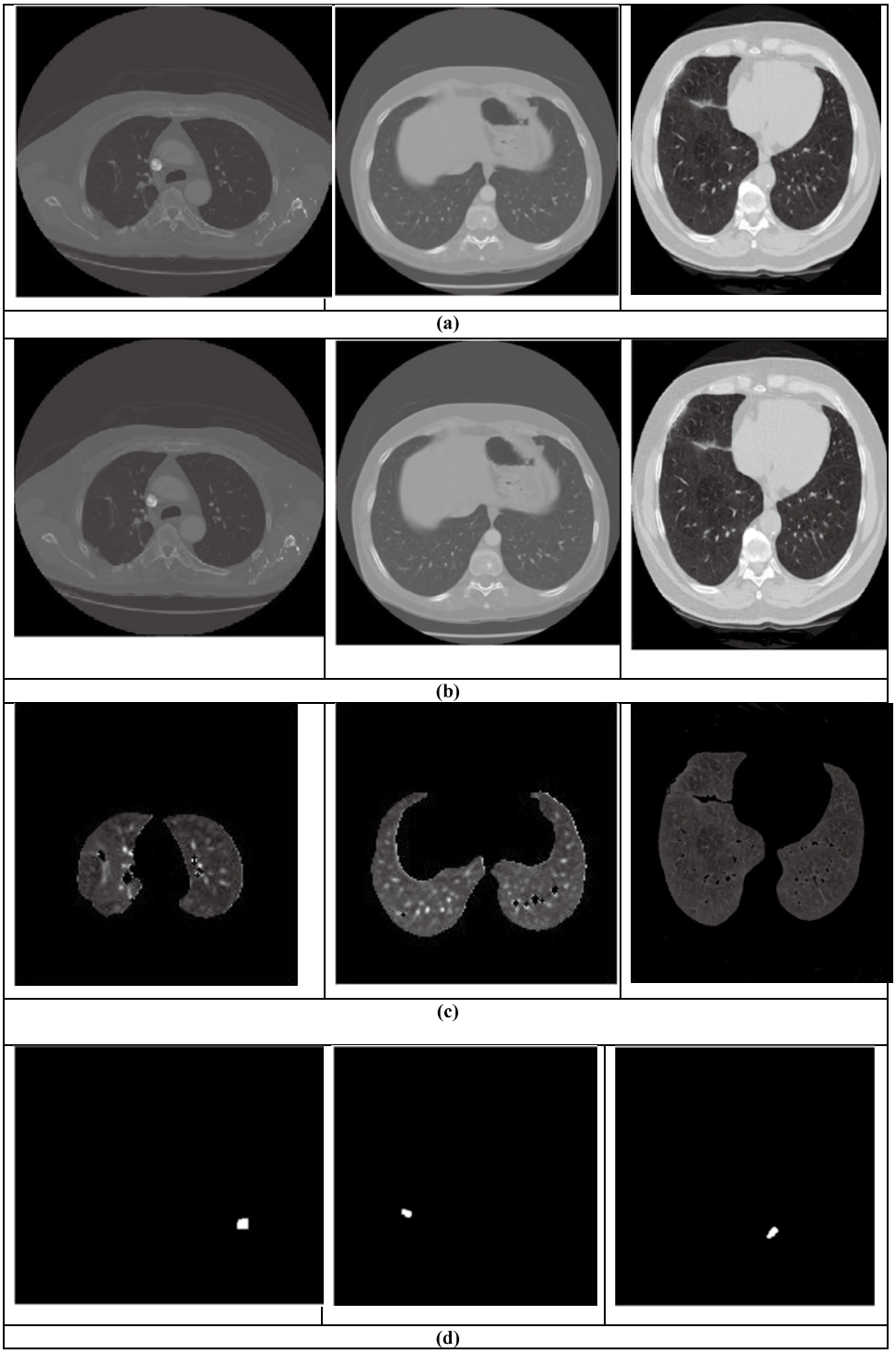

Figure 3. Experimental results of the proposed method : (a) Input images, (b) Filtered images (c) Lobe segmented images and (d) Cancer segmented images.

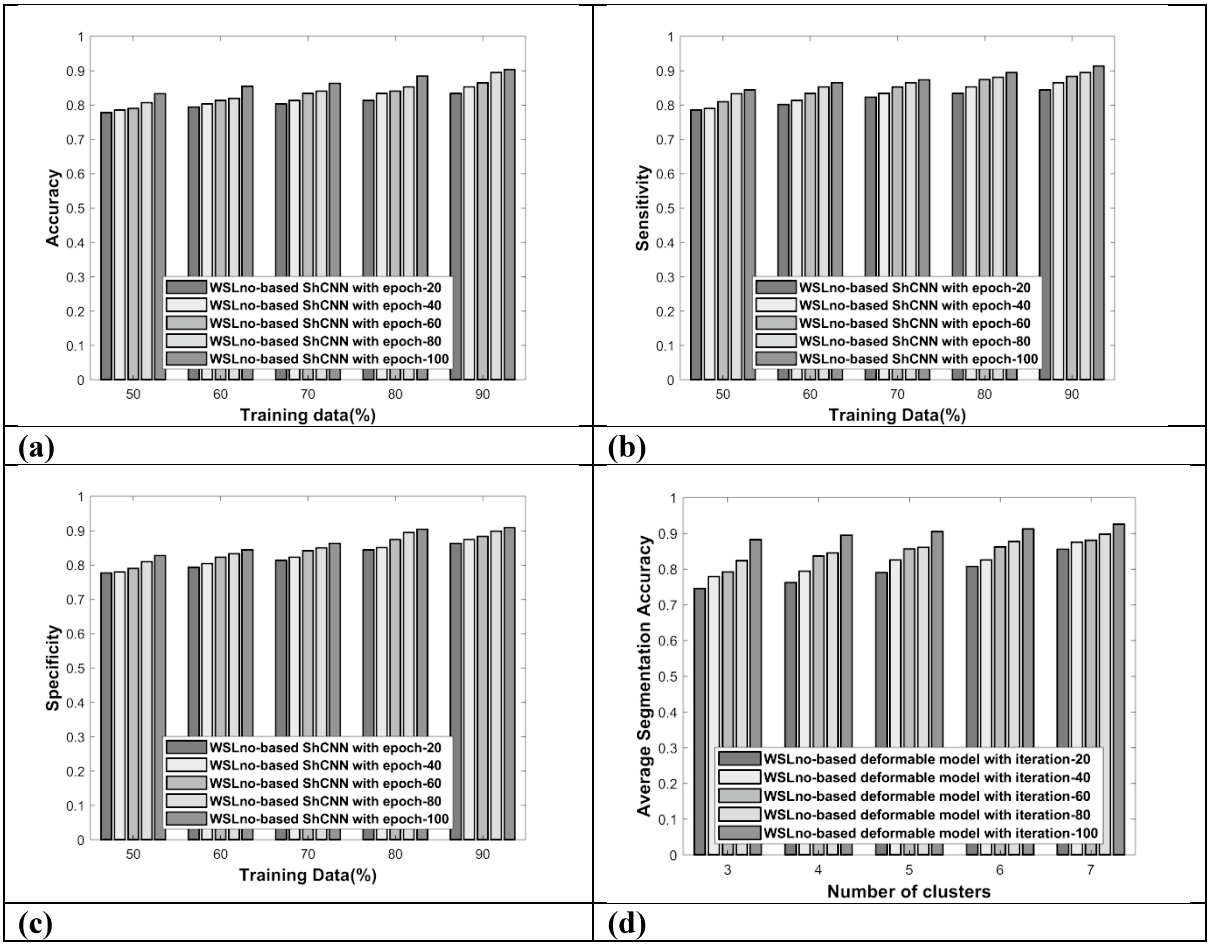

Figure 4. Performance assessment based on training data with different cluster size : (a) Accuracy, (b) Sensitivity, (c) Specificity and (d) Average segmentation accuracy.

4.2 Comparative Analysis

The performance of the proposed WSLnO based deformable model+ShCNN is compared with the existing techniques such as CNN (23), IPCT+NN (24), dictionary based segmentation+ShCNN (18) and WCBA based deformable model+ShCNN (19).

Figure 5 shows the comparative assessment of the proposed method with the existing techniques. For the 60% training data size, the accuracy attained by the proposed method is 0.873, CNN is 0.808, IPCT+CNN is 0.775, Dictionary based segmentation+ShCNN is 0.846 and WCBA-based deformable model+ShCNN is 0.851. Moreover, the percentage improvement obtained by the proposed method based on existing approaches is 7.47 %, 11.29 %. 3.12 % and 2.60 %. For the training data 70%, then the sensitivity obtained by the existing model, like CNN, IPCT+NN, dictionary based segmentation+ShCNN and WCBA based deforma-ble model+ShCNN is 0.823, 0.799, 0.858 and 0.866, whereas the proposed method attained maximum sensitivity of 0.873 as shown in figure 5(b). The percentage improvement obtained by the proposed model based on sensitivity is 6.70%, 8.49%, 3.49% and 1.85%, respectively. In figure 5(c), the specificity of the proposed model is 0.894 for 80% of the training data. Whereas the existing models attained the specificity of 0.844, 0.815, 0.862 and 0.879 respectively. Furthermore, the percentage of improvement is 6.63%, 9.80%, 4.70% and 2.82%. Similarly, figure 5(d) shows the comparative assessment for average segmentation accuracy.

When the cluster count is 6, then the average segmentation accuracy obtained by the proposed model is 0.924, whereas for the existing methods 0.812, 0.848, 0.866 and 0.891 respectively. Also, the percentage improvement by the proposed model is 12.16%, 8.21%, 6.31% and 3.52%. The performance comparison of the proposed method is also evaluated in the presence of various noise as shown in figure 6. When the density of the noise is 0.1, then the accuracy attained by the proposed model is 0.8216, whereas the existing techniques attained the accuracy of 0.7661, 0.7736, 0.7783 and 0.7949 respectively and is depicted in figure 6(a). Furthermore, the percentage improvement obtained by the proposed model relies on accuracy is 6.75%, 5.84%, 5.26% and 3.24%. Similarly, figure 6(b) shows the comparative assessment on average segmentation accuracy by changing the noise density. When the density of the noise is 0.08, then the average segmentation accuracy attained by the existing models are 0.7500, 0.7821, 0.8243, 0.8333 and the proposed model is 0.8821. Also, the performance improvement of the proposed model is 14.97%, 11.33%, 6.55% and 5.53%.

The performance comparison of the proposed model is also tested with salt and pepper noise as shown in figure 7. For the noise density of 0.06, then the accuracy obtained by the existing model is 0.832, 0.7832, 0.8431 and 0.8531, whereas the proposed method is 0.8776. Furthermore, the percentage improvement obtained by the developed model based on accuracy is 5.19%, 10.74%, 3.93% and 2.78%. Similarly, when the noise density is 0.04, then the average segmentation accuracy attained by the proposed model is 0.9122 and for the existing approaches is

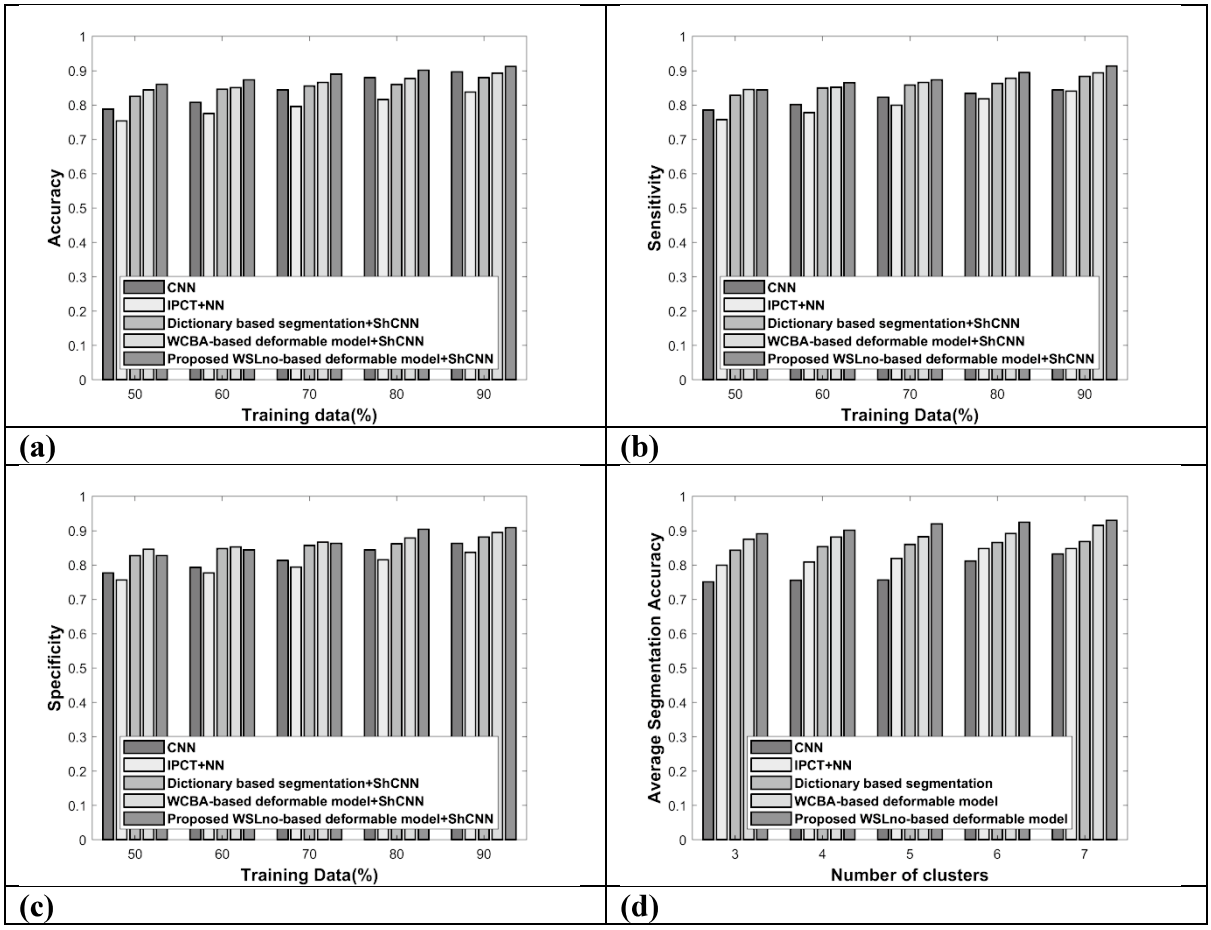

Figure 5. Comparison of the proposed method with the existing models : (a) Accuracy, (b) Sensitivity, (c) Specificity and (d) Average segmentation accuracy.

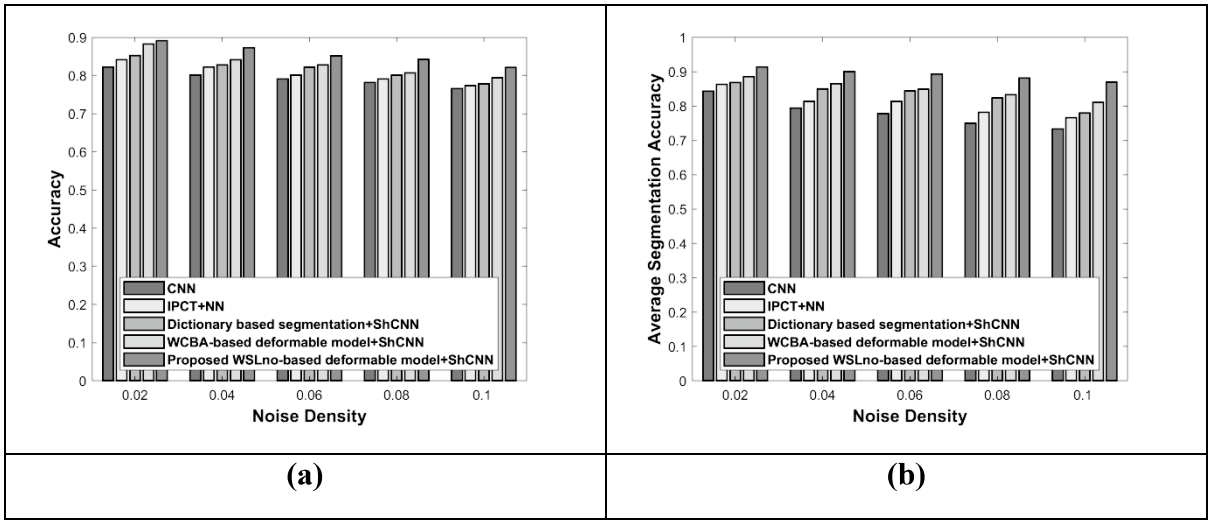

Figure 6. Comparative assessment in the presence of noise : (a) Accuracy for Gaussian noise (0.1) and (b) Average segmentation accuracy for Gaussian noise (0.08).

0.7997, 0.8362, 0.8537 and 0.8795 as shown in figure 7(b). Furthermore, the percentage improvement of the proposed model is 12.33%, 8.32%, 6.40% and 3.57%.

Table 1 shows the quantitative values of the pro-posed method in terms of accuracy, sensitivity, specificity and the average segmentation accuracy as against the existing models. From the table, the proposed model attained the maximum average segmentation accuracy of 0.9303, maximum accuracy of 0.9123, maximum sensitivity of 0.9133 and maximum specificity of 0.9091 respectively as compared to the existing models. Moreover, the existing methods attained the segmentation accuracy of 0.8321, 0.8486, 0.8686 and 0.9152, accuracy of 0.8966, 0.8379, 0.88 and 0.8932, sensitivity of 0.8443, 0.8407, 0.8834 and 0.8937 and specificity of 0.8633, 0.8369, 0.8821 and 0.8947, correspondingly by varying the training data percentage.

CONCLUSION

In this paper, the proposed method is developed and implemented for accurate segmentation and classification of lung cancer using CT images. The deformable model is designed by modifying the dictionary based image segmentation using optimization algorithm. The lung cancer classification is carried out using ShCNN and the weight of ShCNN is trained using proposed WSLnO model. The experimental results shows the improved performance in terms of accuracy, sensitivity, specificity and average segmentation accuracy. The comparative results were also proved the superiority of the proposed method.

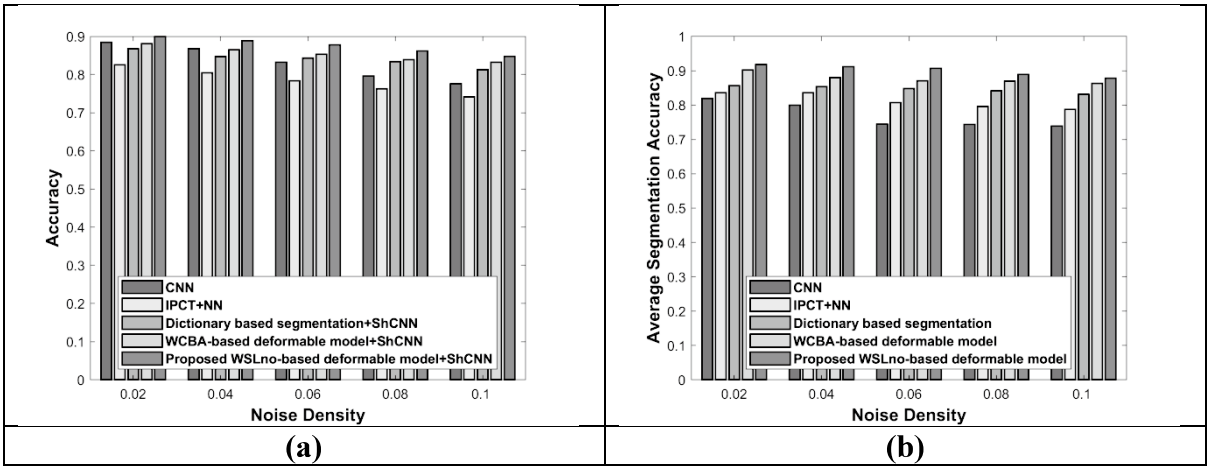

Figure 7. Comparative assessment in the presence of noise: (a) Accuracy for salt and pepper noise (0.06) and (b) Average segmentation accuracy for salt and pepper noise (0.04).

Table 1. Performance comparison of the proposed method with the existing models.

	Metrics	CNN [23]	IPCT+NN [24]	Dictionary based segmentation+ ShCNN [18]	WCBA based deformable model+ShCNN [19]	Proposed Method
Training data	Avg. Segmentation accuracy	0.8321	0.84869	0.8686	0.9152	**0.93034**
	Accuracy	0.8966	0.8379	0.88	0.8932	**0.9123**
	Sensitivity	0.8443	0.8407	0.8834	0.8937	**0.9133**
	Specificity	0.8633	0.8369	0.8821	0.8947	**0.9091**
Gaussian noise	Accuracy	0.7661	0.7736	0.7783	0.7949	**0.8216**
	Average segmentation accuracy	0.7332	0.7663	0.7799	0.8111	**0.8701**
Salt and pepper noise	Accuracy	0.776	0.7416	0.813	0.8326	**0.8476**
	Average segmentation accuracy	0.7387	0.7871	0.8315	0.8628	**0.8784**

REFERENCES

1. Nanglia P, Kumar S, Mahajan AN, Singh P, Rathee D : A hybrid algorithm for lung cancer classification using SVM and Neural Networks. ICT Express 5(3) : 335-341, 2021
2. Park S, Lee SJ, Weiss E, Motai Y : Intra and inter-fractional variation prediction of lung tumors using fuzzy deep learning. IEEE Journal of Translational Engineering in Health and Medicine 4(1) : 1-12, 2016
3. Sharma D, Jindal G : Computer aided diagnosis system for detection of lung cancer in CT scan images. International Journal of Computer and Electrical Engineering 3(5) : 714-718, 2011
4. Shankar KA, De Albuquerque VHC : Optimal feature-based multi-kernel SVM approach for thyroid disease classification. The Journal of supercomputing 76(2) : 1128-1143, 2020
5. Sarker P, Shuvo MMH, Hossain Z, Hasan S : Segmentation and classification of lung tumor from 3D CT image using K-means clustering algorithm. In proceedings of 4th International Conference on Advances in Electrical Engineering (ICAEE) : 731-736, 2017
6. Yang Z, Yang D, Dyer C, He X, Smola A, Hovy E : Hierarchical attention networks for document classification. In Proceedings of the 2016 conference of the North American chapter of the association for computational linguistics : human language technologies : 1480-1489, 2016
7. Jiang H, Ma H, Qian W, Gao M, Li Y : An automatic detection system of lung nodule based on multigroup patch based deep learning network. IEEE Journal of Biomedical and Health Informatics 22(4) : 1227-1237, 2018
8. Chung H, Ko H, Jeon SJ, Yoon KH, Lee J : Automatic lung segmentation with juxta-pleural nodule identification using active contour model and Bayesian approach. IEEE Journal of Translational Engineering in Health and Medicine 6 : 1-13, 2018
9. Riquelme D, Akhloufi MA : Deep learning for lung cancer nodules detection and classification in CT scans. AI 1(1) : 28-67, 2020
10. Yu H, Zhou Z, Wang Q : Deep Learning Assisted Predict of Lung Cancer on Computed Tomography Images using the Adaptive Hierarchical Heuristic Mathematical Model. IEEE Access 8 : 86400-86410, 2020
11. Ozdemir O, Russell RL, Berlin AA : A 3D probabilistic deep learning system for detection and diagnosis of lung cancer using low-dose CT scans. IEEE Transactions on Medical Imaging 39(5) : 1419-1429, 2019
12. Khan MA, Rubab S, Kashif A, Sharif MI, Muhammad N, Shah JH, Zhang YD, Satapathy SC : Lungs cancer classification from CT images : An integrated design of contrast based classical features fusion and selection. Pattern Recognition Letters 129 : 77-85, 2020
13. Suresh S, Mohan S : ROI-based feature learning for efficient true positive prediction using convolutional neural network for lung cancer diagnosis. Neural Computing and Applications 32(20) : 15989-16009, 2020
14. Bonavitaa I, Rafael-Paloua X, Ceresab M, Piellab G, Ribasa V, Ballester MAG : Integration of Convolutional Neural Networks for Pulmonary Nodule Malignancy Assessment in a Lung Cancer Classification Pipeline. Journal of Computer Methods and Programs in Biomedicine 185 : 1-9, 2019
15. Chilakala LR, Kishore GN : Optimal deep belief network with opposition-based hybrid grasshopper and honeybee optimization algorithm for lung cancer classification : A DBNGHHB approach. International Journal of Imaging Systems and Technology 31(3) : 1404-1423, 2021
16. Lakshmanaprabu SK, Mohanty SN, Shankar K, Arunkumar N, Ramirez G : Optimal deep learning model for classification of lung cancer on CT images. Future Generation Computer Systems 92 : 374-382, 2019
17. Glenn TC, Zare A, Gader PD : Bayesian Fuzzy Clustering. IEEE Transactions on Fuzzy Systems 23(5) : 1545-1561, 2015
18. Dahl AB, Dahl VA : Dictionary based image segmentation. In Scandinavian conference on image analysis : 26-37, 2015
19. Eskandar H, Sadollah A, Bahreininejad A, Hamdi M : Water cycle algorithm–A novel metaheuristic optimization method for solving constrained engineering optimization problems. Computers and Structures 110 : 151-166, 2012
20. Masadeh R, Mahafzah BA, Sharieh A : Sea lion optimization algorithm. International Journal of Advanced Computer Science and Applications 10(5) : 388 -395, 2019
21. Ren JS, Xu L, Yan Q, Sun W : Shepard convolutional neural networks. Advances in Neural Information Processing Systems 28 : 901-909, 2015
22. Lung Image Database Consortium image collection (LIDC-IDRI) dataset, "https://wiki.cancerimagingarchive.net/display/Public/LIDC-IDRI", accessed on February 2020
23. Hu Q, Souza LFDF, Holanda GB, Alves SS, Silva FHDS, Han T, Reboucas Filho PP : An effective approach for CT lung segmentation using mask region-based convolutional neural networks. Artificial Intelligence in Medicine 103 : 101792, 2020
24. Shakeel PM, Burhanuddin MA, Desa MI : Lung cancer detection from CT image using improved profuse clustering and deep learning instantaneously trained neural networks. Measurement 145 : 702-712, 2019